










Electrocatalytic and stoichiometric reactivity of 2D layered siloxene for high-energy-dense lithium–sulfur batteries

Hui-Ju Kang¹  | Jae-Woo Park¹  | Hyun Jin Hwang¹  | Heejin Kim²  | Kwang-Suk Jang³  | Xiulei Ji⁴  | Hae Jin Kim²  | Won Bin Im⁵  | Young-Si Jun¹ 

¹Department of Advanced Chemicals & Engineering, Chonnam National University, Gwangju, Republic of Korea

²Division of Analytical Science, Korea Basic Science Institute (KBSI), Daejeon, Republic of Korea

³Department of Applied Chemistry, Hanyang University, Ansan, Gyeonggi-do, Republic of Korea

⁴Department of Chemistry, Oregon State University, Corvallis, Oregon, USA

⁵Division of Materials Science and Engineering, Hanyang University, Seoul, Republic of Korea

Correspondence

Heejin Kim, Division of Analytical Science, Korea Basic Science Institute (KBSI), Daejeon 34133, Republic of Korea.
Email: heejinkim@kbsi.re.kr

Won B. Im, Division of Materials Science and Engineering, Hanyang University, 222 Wangsimni-ro, Seongdong-gu, Seoul 04763, Republic of Korea.
Email: imwonbin@hanyang.ac.kr

Young-Si Jun, Department of Advanced Chemicals & Engineering, Chonnam National University, 77 Yongbong-ro, Buk-gu, Gwangju 61186, Republic of Korea.
Email: ysjun@jnu.ac.kr

Funding information

National Research Council of Science and Technology, Grant/Award Number: CAP-15-02-KBSI; National Research Foundation of Korea, Grant/Award Numbers: 2019R1A4A2001527, 2019R1C1C1007745

Abstract

Lithium–sulfur batteries (LSBs) have emerged as promising power sources for high-performance devices such as electric vehicles. However, the poor energy density of LSBs owing to polysulfide shuttling and passivation has limited their further market penetration. To mitigate this challenge, two-dimensional (2D) siloxene (2DSi), a Si-based analog of graphene, is utilized as an additive for sulfur cathodes. The 2DSi is fabricated on a large scale by simple solvent extraction of calcium disilicide to form a thin-layered structure of Si planes functionalized with vertically aligned hydroxyl groups in the 2DSi. The stoichiometric reaction of 2DSi with polysulfides generates a thiosulfate redox mediator, secures the intercalation pathway, and reveals Lewis acidic sites within the siloxene galleries. The 2DSi utilizes the corresponding in-situ-formed electrocatalyst, the 2D confinement effect of the layered structure, and the surface affinity based on Lewis acid–base interaction to improve the energy density of 2DSi-based LSB cells. Combined with the commercial carbon-based current collector, 2DSi-based LSB cells achieve a volumetric energy density of 612 Wh L_{cell}^{−1} at 1 mA cm^{−2} with minor degradation of 0.17% per cycle, which rivals those of state-of-the-art LSBs. This study presents a method for the industrial production of high-energy-dense LSBs.

KEYWORDS

2D confinement effects, Lewis acid–base interactions, lithium–sulfur batteries, siloxenes, thiosulfate–polythionate redox couple

This is an open access article under the terms of the Creative Commons Attribution License, which permits use, distribution and reproduction in any medium, provided the original work is properly cited.

© 2021 The Authors. *Carbon Energy* published by Wenzhou University and John Wiley & Sons Australia, Ltd.

1 | INTRODUCTION

Electric vehicles and grid-scale energy storage systems require batteries to power them for their widespread applications. The current state-of-the-art battery technology is lithium-ion batteries (LIBs), the performance of which is, however, already close to the theoretical limits (240–460 Wh kg⁻¹ and 640 Wh L⁻¹)^{1–3} and the cost reduction of which progresses slowly (~\$100 kWh⁻¹).⁴ To make electric vehicles competitive with gasoline cars, batteries need to be improved in terms of energy density (greater than 400 Wh kg⁻¹ and greater than 600 Wh L⁻¹), power density (1000 W kg⁻¹ and 2000 W L⁻¹),^{3,5,6} cycle stability (greater than 1000 cycles), safety, and cost (less than \$100 kWh⁻¹). Such demands have led to research on lithium–sulfur batteries (LSBs) based on an electrochemical reaction between lithium and sulfur to form Li₂S. LSBs not only show a high energy density (~2500 Wh kg⁻¹ and ~2800 Wh L⁻¹) due to their chemistry but also use inexpensive, abundant, and ecofriendly sulfur as an active material. Moreover, the manufacturing process of LSBs can adapt to that of LIBs without significant modifications.⁷

With the same dimensions of the cell components, LSBs must have an areal capacity higher than that of the commercial LIBs (~4 mAh cm⁻²) to effectively replace LIBs in high-performance devices.^{8,9} In addition, given the operating potential of 2.1 V versus Li/Li⁺, the capacity of LSBs needs to be at least doubled as compared to that of LIBs with a working potential of 3.5–4.0 V versus Li/Li⁺. Assuming a sulfur-utilization efficiency of 60%–80%, this, in turn, requires an areal sulfur loading of 6–8 mg cm⁻². However, despite the vast amount of research on every aspect of batteries, including a cathode, anode, separator, binder, and electrolyte, such high requirements in areal sulfur loading only emerged recently.¹⁰ Researchers have paid considerable attention to mitigating polysulfide shuttling at a low areal sulfur loading of ~2 mg cm⁻². A question arises as to whether or not these strategies are still valid under the high areal sulfur-loading conditions (i.e., greater than 6 mg cm⁻²). Growing concerns stem from the simple calculation that, assuming a utilization efficiency of less than 60% typical for the high-sulfur-loading conditions, the sulfur loss mostly into the electrolyte corresponds to greater than 2.4 mg cm⁻², exceeding the low-sulfur-loading conditions. Under the high loading conditions, it is reasonable to believe that the polysulfide shuttling is intensified enough to neutralize the strategies suggested in the low loading conditions.^{11,12} Manthiram et al.¹³ demonstrated that high-sulfur-loading conditions (in the range of 6–61.4 mg cm⁻²) induce substantial passivation of a Li metal anode with Li₂S even in the presence of a highly

efficient porous carbon supporting material. In particular, Li₂S passivation will be a huge concern when using a stoichiometric amount of Li metal anode, which is crucial for achieving high-energy-dense LSBs.¹⁴ This justifies further research efforts and demands for high-sulfur-loading systems.

To alleviate the highly intensified polysulfide shuttling as well as the intrinsic insulating property of sulfur, high-sulfur-loading LSB cells (or cathodes) still require porous conductive supporting material.¹⁵ Conductive supporting materials must have a large pore size (greater than 10 nm) and high specific pore volume (greater than 2 cm³ g⁻¹) to efficiently accommodate a large amount of sulfur and its volume expansion by 180% during repeated charge/discharge cycles. However, such large pores are prone to substantial polysulfide shuttling due to the decreased physical confinement effect: At large pore size ranges, the interaction between polysulfides and the pore wall of the conductive supporting material becomes negligible, and thus, this pore size will have no significant effect on the diffusive transport of polysulfides.¹⁶ This suggests that high-sulfur-loading cathodes need to be supplemented with additives (or functionalities) that can provide a strong affinity to polysulfides and, if possible, facilitate their redox reactions quickly toward the ultimate insoluble products, that is, Li₂S_x (x ≤ 2). Various potential additives have been introduced including transition-metal carbides/nitrides/oxides with a polar surface, carbonaceous materials modified with polysulfide-philic N-, O-, and S-heteroatoms, MXenes, and metal–organic frameworks with Lewis acidic metal sites.^{17–19} Previous studies have reported that these functional materials enable highly efficient polysulfide retention via chemical adsorption with a low concern of nanostructure. Moreover, some of these functional materials with a redox potential between 2.4 and 3.05 V versus Li/Li⁺ or surface hydroxyl groups are also capable of mediating thiosulfate formation in the presence of polysulfides. These in-situ-formed insoluble thiosulfate species further strengthen the chemical adsorption of polysulfides by forming a polythionate complex, thus significantly enhancing the cycle stability.^{20,21}

However, despite the promising capability to retain polysulfides, it is still unclear whether these chemical adsorption-based surface strategies can be successfully implemented at high-sulfur-loading cathodes. Moreover, most of these studies were performed under relatively low-sulfur-loading conditions (less than 6 mg cm⁻²). This can be attributed to the fact that chemical adsorption functions only at or near the interface between the host matrix and the electrolyte. In addition, similar to physical confinement, these strategies require the delicate control of the pore structure to maximize the adsorption sites while minimizing its content. In particular, the contents

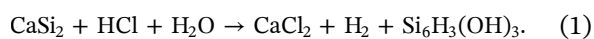
of inactive materials including the sulfur host and additives are strictly limited (less than 30 wt%) for achieving high-energy-dense LSBs. Moreover, the tailoring or large-scale production of these functional materials has a significant impact on the environment.^{19,22,23} Therefore, we explored new multifunctional additives that can be easily tailored, be produced on a large scale, and function efficiently under high-sulfur-loading conditions.

Herein, we propose a novel strategy for solving the technical challenges of immobilizing lithium polysulfides by utilizing two-dimensional layered siloxene (2DSi) as a multifunctional cathode material. The 2DSi possesses attractive structural characteristics. For example, its 2D layers are stacked at a constant interval (0.53 nm), and it possesses hydroxyl functional groups in the direction perpendicular to the skeleton of silicon, which is appropriate for aligning linear lithium polysulfide molecule species into the interlayers and for maintaining the interaction between lithium polysulfides and 2DSi. In addition, a rich hydroxyl (or oxygen) functional group was formed in the 2DSi to form a highly polysulfide-philic surface, which can increase the wettability of the 2DSi with an organic electrolyte and enable reversible adsorption such as oxygen with lithium cation and silicon with polysulfide anion and the stoichiometric reactivity of the 2DSi, thus inducing the in-situ formation of the polysulfide redox mediator thiosulfate. Moreover, these structural properties not only conferred high tortuosity to the lithium polysulfide diffusing pathway from the cathode to the organic electrolyte but also enabled the maintenance of an excellent cycling performance under high-sulfur-loading conditions. We demonstrated that the polysulfide trapping ability (7.49 mAh cm⁻² at 1 mA cm⁻²) of the additive material can be retained for 200 cycles with a large average Coulombic efficiency of 97% under a high-sulfur-loading condition (10 mg S cm⁻²). The enhanced electrochemical performance indicates the effectiveness of the aromatic silicon-based hydroxyl (or oxygen) functional group-containing 2D material for achieving a high-sulfur-loading cathode with a high utilization efficiency of 44.8%.

2 | EXPERIMENTAL SECTION

2.1 | Synthesis of 2DSi

Removal of calcium from calcium disilicide (Ca; 30%–33%, Si; 60%–62%, CaSi₂; Sigma-Aldrich) was achieved by simple solvent extraction according to the following chemical equation:



CaSi₂ (20 g) was treated with a high-concentrated hydrochloric acid at room temperature (RT) under a N₂ atmosphere overnight (12 h). Special precautions are required to prevent explosions due to massive hydrogen evolution. The yellow-green powder was recovered after filtering, washing with acetone, and finally drying the slurry at 80°C under vacuum. The resulting siloxene (Si₆H₃(OH)₃) is referred to as 2DSi. All chemicals were used without additional purification.

2.2 | Electrochemical measurements

2DSi electrodes were prepared using the slurry casting method. For slurry preparation, 2DSi powder (70 mg), Super P (20 mg), and poly(vinylidene difluoride) (PVdF) binder (10 mg) were dispersed in *N*-methyl-2-pyrrolidone (NMP). The homogeneous mixture was obtained after sonicating for 3 h and stirring overnight. The resulting uniform slurry solution was cast onto carbon cloth (CC) or carbon nanotube (CNT) bucky paper and then dried in a vacuum oven at 120°C for 24 h. The areal loading of 2DSi on CC (or CNT paper) was estimated to be about 2–6 mg cm⁻². Details of CC and CNT are given in the Supporting Information Materials.

The cell was assembled in an Ar-filled glovebox with impure oxygen and H₂O less than 0.1 ppm. 2DSi on CC (or CNT paper; 2DSi/CC, 2DSi/CNT), a Celgard 2000 membrane (19 mm), and a lithium metal foil (Ø: 10 mm, thickness: 0.75 mm) were used as the working electrode, separator, and counter electrode, respectively. These cell components were all sealed in a CR2032 coin cell using a manual coin cell crimper. We added a stainless-steel current collector and spring to the lithium metal disc to maintain the electrical contact between the lithium metal and the negative cell case during electrochemical characterization. The electrolyte used was 1 M lithium bis(trifluoromethanesulfonyl)imide (LiTFSI) with 1 wt% LiNO₃ dissolved in 1,3-dioxolane (DOL) and 1,2-dimethoxyethane (DME) (1:1, volume/volume). The sulfur source was 1 M Li₂S₆ dissolved in the electrolyte. The catholyte was prepared according to the method described elsewhere.²⁴ Depending on the target areal sulfur loading (2–10 mg sulfur cm⁻²), a different amount of the catholyte solution was applied to the 2DSi/CC electrode. Then, we added different amounts of the electrolyte solution to the membrane separator to maintain the ratio of (electrolyte and catholyte) volume to sulfur weight of 13 μL mg⁻¹. Galvanostatic cycling using the potential limitation (GCPL) technique was carried out on the WBCS3000S (WonATech) in the potential range between 1.8 and 2.6 V versus Li/Li⁺ at

different areal current densities (1–4 mA cm⁻²). Cyclic voltammetry (CV) at a scanning rate of 0.01 mV s⁻¹ within the potential range of 1.0–3.0 V versus Li/Li⁺ and electrochemical impedance spectroscopy measurements with the frequency range of 500 kHz–0.05 Hz were conducted on a VSP potentiostat (Bio-logic). Both specific capacity and current density were calculated based on the area of the cathode (1.54 cm²).

3 | RESULTS AND DISCUSSION

3.1 | Structural characterization of 2DSi

Among several stable Zintl silicides, calcium disilicide (CaSi₂) is the only compound that contains interconnected six-membered rings of Si atoms. These rings are extended into the 2D layers and thus form an anionic corrugated sheet-like structure held together by alternating layers of Ca²⁺ similar to graphite²⁵ (Figure 1A). In addition, the covalent Si–Si bonds can remain stable

under harsh conditions, thus enabling the large-scale synthesis of a Si-based sheet-like structure full of Lewis acidic sites via a simple solvent extraction of Ca²⁺.²⁶ Furthermore, controlled chemical modification of the Si skeleton can be simultaneously achieved by simply changing the Ca²⁺ extraction temperature (–20°C to 25°C), the introduction of thiosulfate-mediating hydroxyl groups by which is the aim of this study.

As shown in the X-ray photoelectron spectroscopy (XPS) survey spectra (Figure S1 and Table S1), the Ca²⁺ extraction process reduced the Ca content of the CaSi₂ from 9.8 at% to less than 1.3 at% and reduced the Ca/Si molar ratio from 0.57 to 0.03, indicating the substantial removal of Ca²⁺ binding layers in the CaSi₂ by the simple solvent extraction method. This result is further confirmed by the complete disappearance of the CaSi₂ characteristic peaks at 17.3°, 26.8°, 33.8°, 39.9°, and 42.3° in the powder X-ray diffraction (XRD) pattern of CaSi₂ (Figure S2a), corresponding to (0 0 1), (1 0 1), (1 0 7), (1 0 10), and (0 1 11) reflections (JCPDS No. 01-075-2192), respectively.²⁷ In addition, a layered structure with

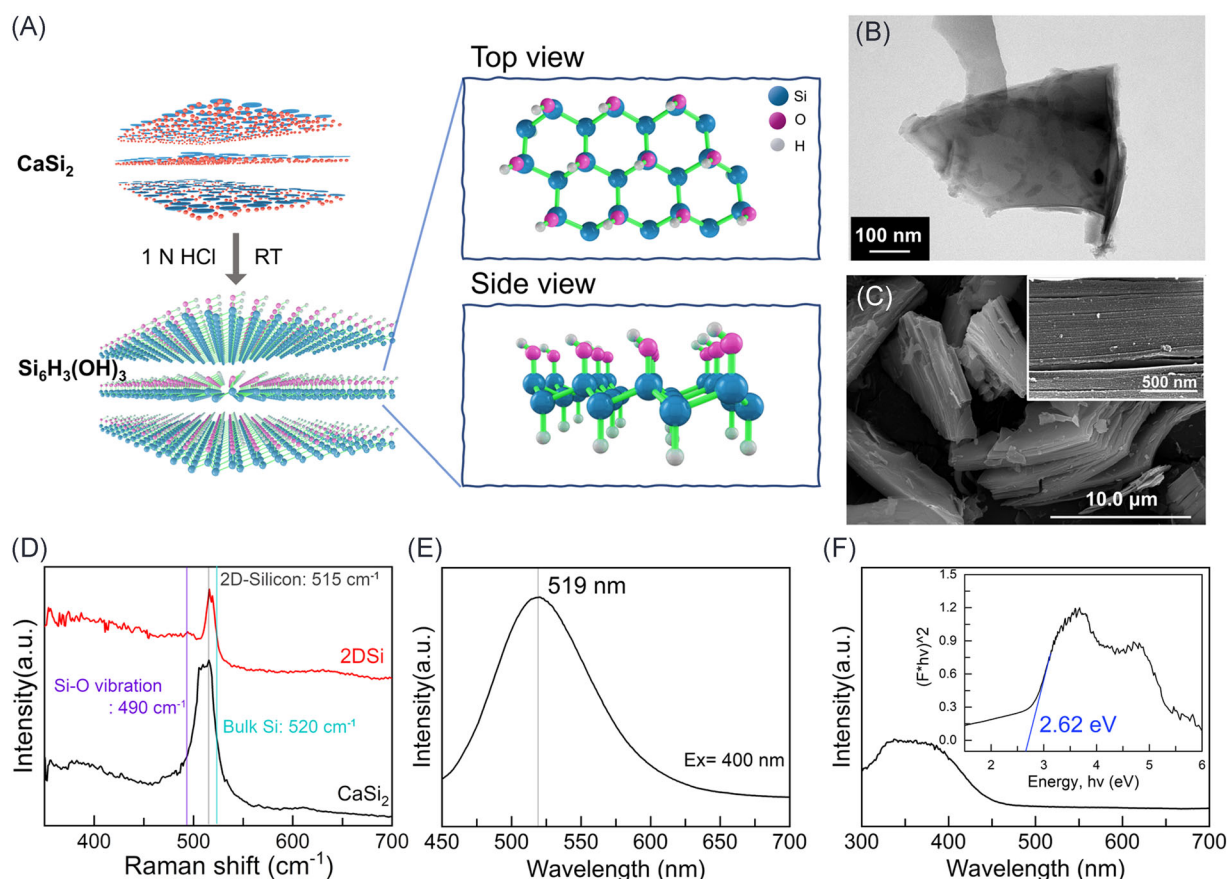


FIGURE 1 2DSi: (A) Schematic description of the solvent extraction and the resulting chemical structure, (B) TEM image, (C) SEM image with an inset image of higher magnification, (D) Raman spectra, (E) PL spectra, and (F) DRS UV-vis spectra with an inset of the Tauc plot. 2DSi, two-dimensional siloxene; DRS, differential reflectance spectroscopy; PL, photoluminescence; SEM, scanning electron microscopy; TEM, transmission electron microscopy

parallel planes was observed after the removal of Ca^{2+} , which emerged from the smooth-surfaced polygonal crystals of CaSi_2 (Figures 1B and S3a). The estimated interlayer spacing between the 2D graphite-like layers is approximately 0.53 nm, with a moderate-intensity peak at 17.3° in the XRD pattern corresponding to the (0 0 1) reflection (Figure S2b).

The transparent particles shown in the TEM images indicate that the 2DSi consists primarily of few-layer (or thin) nanosheets with a lateral dimension of less than 500 nm much smaller than that of pristine CaSi_2 particles (100–500 μm) (Figure 1B). In addition, these nanosheets maintain their graphite-like stacked structure at relatively low temperatures (25°C). Note that the graphite oxide is substantially exfoliated via thermal expansion, which requires a temperature as high as 900°C at a fast heating rate.²⁸ Only a part of the plate-like particles of 2DSi is exfoliated, while the rest is divided into smaller pieces during the hydrogen evolution between adjacent layers, which is immediately initiated with heat generation after the addition of an aqueous HCl solution to the CaSi_2 powders. In addition, the reaction is accompanied by a substantial volume expansion of the powder approximately three times, and a change in the powder color from dark gray to yellow-green (Figure S3b). This can be attributed to the fact that the nanosheets are, in part, held by intermolecular interactions such as van der Waals forces or hydrogen bonding, indicating the introduction of surface-functional groups (hydroxyl group).²⁹ In addition, this can also be partly attributed to the prevention of the exfoliation of the stacked nanosheets by the remaining Ca^{2+} bridge³⁰ (Figure 1C).

The in-plane crystal structure of the $(\text{Si}_n)^{2-}$ sheets in the parent CaSi_2 is well preserved in the 2DSi. A dominant peak is observed at 515 cm^{-1} in the Raman spectrum of the 2DSi (Figure 1D), and a broad peak is observed in the range between 380 and 410 cm^{-1} , which is similar to that of CaSi_2 .³¹ However, the slight shift of the Raman spectra of the 2DSi in comparison to that of CaSi_2 can be attributed to the weak interlayer bonding of the 2DSi. The peaks observed in the Raman spectrum of the 2DSi can be assigned to the 2DSi planes rather than to its oxidation products (i.e., Si rings [470 cm^{-1}] or chains [broad peak at 482 cm^{-1}]), indicating that the oxidation that occurred in the 2DSi is marginal even after the harsh chemical extraction. This is consistent with the fact that the 2DSi planes are more stable against thermal or chemical oxidation than Si rings or chains³² (Scheme S1). In addition, a peak is observed at 519 nm in the yellow-green photoluminescence (PL) spectrum of 2DSi (Figure 1E), which can be assigned to the 2DSi planes, whereas the emission peak of Si rings/chains-based Si materials is observed above 540 nm .^{31,32} Furthermore, a highly ordered Si-based crystal lattice is observed in

the high-resolution TEM images and selected area electron diffraction (SAED) pattern (Figure S4): 2DSi has a lattice parameter of 0.317 nm in the a -direction similar to that of siloxene (chemical structure, $\text{Si}_6\text{H}_3(\text{OH})_3$, with $a_{\text{hex}} = 0.333 \pm 0.018\text{ nm}$).^{33,34} Such an ordering prevails over the samples, as supported by a strong XRD peak at 28.5° corresponding to the (1 0 0) reflection with a d_{100} of 0.312 nm (Figure S2c). These lattice parameters of TEM and XRD analyses are consistent with those reported in previous studies.³³ Therefore, we ensure the selective removal of the Ca^{2+} interlayer by the chemical extraction, while maintaining the characteristic crystal structure of the corrugated Si (1 1 1) plane of CaSi_2 , which is crucial for fully exposing the Lewis acidic Si sites on 2DSi.³¹

2DSi is a semiconductor based on sp^3 -hybridized Si that is more energetically favored than the semimetallic sp^2 -hybridized Si.³³ On the basis of the linear fitting of the absorption edge of the Tauc plot, the optical band gap of the 2DSi is estimated to be approximately 2.62 eV (Figure 1F), which is consistent with the theoretical value (2.75 eV) of hydride terminated silicane or layered polysilane.³⁵ Owing to the sp^3 coordination of a Si atom, it is presumed that all of the Si atoms of Si planes contain either H or OH termination. The OH termination content, which is beneficial for the formation of the thiosulfate redox mediator, can be increased by increasing the extraction temperature.^{21,29} Weiss et al. suggested that one of the siloxene derivatives prepared at a moderate temperature such as 0°C consists essentially of Si planes terminated by alternating H and OH, that is, $\text{Si}_6\text{H}_3(\text{OH})_3$.³⁶ Therefore, we performed the extraction at an elevated temperature (20 – 25°C) to increase the content of the surface OH terminal groups. The XPS survey scan indicates that the surface oxygen content of the 2DSi is as high as $45.6\text{ at}\%$, confirming the introduction of a large amount of surface OH groups. The presence of Si–OH (103 eV), Si–O (108 eV), Si–O–Si (532 eV), and Si–OH (536 eV) bonds is revealed in the high-resolution XPS Si 2p (Figure S1c) and O 1s (Figure S1d) spectra. The FT-IR spectrum (Figure S5) also identifies several Si–H and Si–OH modes in the 2DSi similar to those found in Wohler or Weiss siloxene: Si–H bending at 640 cm^{-1} , Si–H stretching at 2100 cm^{-1} , Si–H₂ wagging and scissors in the range between 835 and 870 cm^{-1} , O–H bending at 1620 cm^{-1} , and O–H stretching in the range between 3400 and 3580 cm^{-1} . Partial insertion of oxygen into 2DSi planes is also seen by the Si–O–Si stretching mode at 1050 cm^{-1} and O–Si–H stretching at 2200 cm^{-1} . The single peak structure of the former confirms the low oxidation level of the 2DSi plane, while the latter corresponding to the Si–H back-bonded by O reveals the vertical alignment.³¹

3.2 | Intercalation capability of the 2DSi toward sulfur and high polysulfides

The 2DSi powder showed a negligible Brunauer–Emmett–Teller (BET) surface area of $7 \text{ m}^2 \text{ g}^{-1}$ and a pore volume of $0.007 \text{ cm}^3 \text{ g}^{-1}$ (Figure S6), suggesting expanded roles of 2DSi more than conventional additives under high-sulfur-loading conditions. One possibility is the partial intercalation of polysulfides and lithium ions into the galleries between the siloxene layers. Given the interlayer distance (0.53 nm) and siloxene layer thickness (0.44 nm), the intercalation of elemental sulfur (eight-membered ring structure of 0.546–0.687 nm) or linear polysulfides (e.g., Li_2S_6 of 0.534–0.596 nm) into the 2DSi is still ambiguous.^{37,38} Recent publications, however, imply that a high surface area and a large pore size (or a large interlayer distance) may not be sufficient for intercalation of sulfur species: Carbon zeolite (pore size: 0.46 nm, BET surface area: $876 \text{ m}^2 \text{ g}^{-1}$, pore volume: $0.93 \text{ cm}^3 \text{ g}^{-1}$, and sulfur uptake: 40–60 wt%),³⁹ graphite oxide (interlayer space: 0.35 nm, sulfur uptake: 52 wt %),⁴⁰ and layered double hydroxides ($\text{MgAl-NO}_3\text{-LDH}$, interlayer space: 0.32 nm, BET surface area: $10 \text{ m}^2 \text{ g}^{-1}$, sulfur uptake: 30 wt%)⁴¹ showed infiltration and intercalation behavior of sulfur species into the small micropores and interlayers, respectively. These studies suggest that large elemental sulfur (or high polysulfides) can be broken down into shorter sulfur species (S_x^{2-} , $2 \leq x \leq 6$)

that (1) feature a flat-lying arrangement in the layers, (2) remain stable when confined in the interlayer space, and (3) allow further (electro-)chemical reactions. These findings motivated us to attempt intercalation reactions in the 2DSi.

Surprisingly, the 2DSi allows the intercalation of sulfur into the interlayer space. For the intercalation reaction, the 2DSi was impregnated with a sulfur solution in carbon disulfide, after which the excess sulfur on the surface or in the interstitial space between the 2DSi particles is removed by an additional washing procedure with pure carbon disulfide. The amount of intercalated elemental sulfur is estimated by thermogravimetric analysis (TGA) to be approximately 7.51 wt%, which is lower than that of the intercalation uptake (30 wt%) of $\text{MgAl-NO}_3\text{-LDH}$, which can be attributed to the smaller interlayer distance of the 2DSi due to its layer thickness (Figure 2A). This result translates into a sulfur uptake capability of 0.04305 cm^3 per 1 g of 2DSi (see Calculation S1), which is significantly higher than the pore volume ($0.007 \text{ cm}^3 \text{ g}^{-1}$) of 2DSi. This suggests that the intercalation of sulfur species into the interlayer is higher than the surface adsorption of the pores. The absence of the multiple crystalline (elemental) sulfur peaks in the XRD pattern of the resulting 2DSi confirms the homogeneous distribution of sulfur within the layers (Figure S7). In addition, the interlayer distance and intensity of the (1 0 0) reflection at 28° slightly increased, further

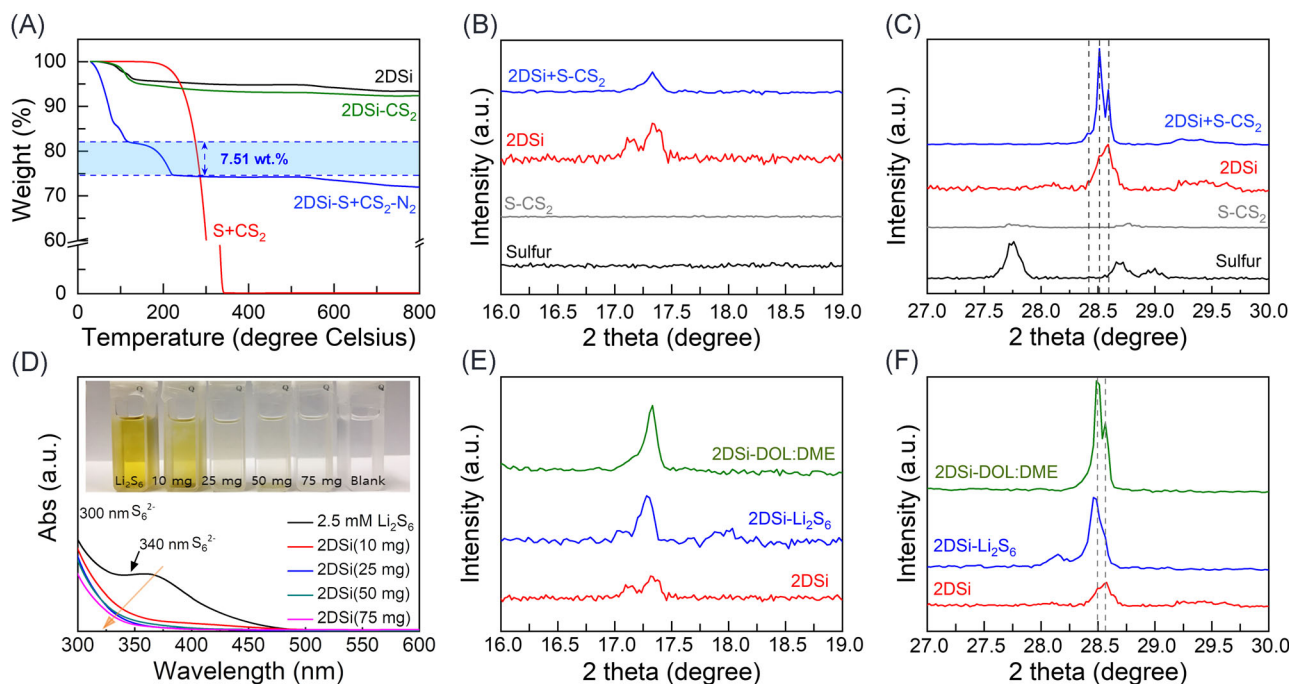


FIGURE 2 Sulfur-infiltrated 2DSi: (A) TGA curves and (B,C) XRD patterns. Li_2S_6 -infiltrated 2DSi: (D) UV-Vis spectra of the 2DSi-treated Li_2S_6 solution (2.5 mM, 10–75 mg 2DSi) and (E,F) XRD patterns. 2DSi, two-dimensional siloxene; TGA, thermogravimetric analysis; XRD, X-ray diffraction

confirming the intercalation of sulfur into the galleries (Figure 2B,C). Furthermore, the interlayer space of the 2DSi could accommodate polysulfides, which is confirmed by the XRD results. To investigate this, 1 M Li_2S_6 dissolved in 1 M LiTFSI-DOL:DME (1:1, volume/volume) was infiltrated into the 2DSi, to directly simulate the polysulfide trap capability of the 2DSi (Figure S8). The peak intensity in the UV-Vis spectrum of the 2DSi in the range between 340 and 360 nm, which corresponds to S_6^{2-} , gradually decreases with an increase in the content of the 2DSi powder and finally becomes negligible when the 2DSi content is higher than 25 mg (Figure 2D).⁴² The almost complete removal of the peak indicates the specific affinity of the 2DSi to polysulfides based on chemisorption rather than physisorption reaching an equilibrium. Notably, the 2DSi powder preserved its layered structure with or without infiltration of sulfur species, as evident from the intact (0 0 1) peak in the powder XRD pattern of the 2DSi (Figure 2E). In addition, unlike typical 2D materials, the 2DSi hardly underwent re-stacking or structure collapse induced by guest molecules, which lead to the substantial loss of the intrinsic properties of the 2D material.²⁴ These results suggest that the layered structure of the 2DSi, resulting from Ca^{2+} extraction, can accommodate sulfur species within the interlayer space. In addition, the layered structure acts as a physical confinement to 2DSi after consuming the surface-functional groups by reacting with sulfur or polysulfides to secure the intercalation pathway. In addition, the abundant internal Si-based Lewis acidic sites and surface-functional groups on the layered 2DSi are easily accessible by polysulfides and exert strong attractive forces on the polysulfides. Furthermore, the hydrogen evolution during Ca^{2+} extraction may further secure the transport paths for electrolyte and sulfur species.

3.3 | Electrochemical characterization of the 2DSi-based LSB cells

The electrochemical characterization of 2DSi in LSBs was performed by loading 2DSi particles on a carbon cloth (2DSi/CC). Carbon cloth (CC) is used as a free-standing sulfur supporting material and as a current collector. The CC efficiently generated polysulfides owing to its high surface area and uniform micropores of approximately 1.1 nm.⁴³ For example, the CC (20 mg cm^{-2}) generates a capacity of 2.5 mAh cm^{-2} from the higher plateau (Figure S9a) at an areal sulfur loading of 10 mg S cm^{-2} and a current density of 1 mA cm^{-2} . This corresponds to a high polysulfide utilization efficiency of 61.4%, under the assumption of an ideal capacity of 4.07 mAh cm^{-2} for the higher plateau (Figure S9 and Calculations S2). Moreover,

the CC is prone to passivation at an areal sulfur loading of over 6 mg cm^{-2} and a current density of 1 mA cm^{-2} . This precludes further reduction and thereby provokes polysulfide shuttling, resulting in a poor total sulfur utilization efficiency of 23.9% and significant capacity degradation after 77 cycles (Figure S9 and Calculation S2). The capacity ratio of the lower plateau to the higher plateau is approximately 0.72, indicating that the capacity generation is primarily initiated from the reaction of the high polysulfides rather than from the low ones. Note that the ideal ratio is 3.⁴⁴ Therefore, we chose CC as the model substrate to investigate the role of 2DSi in suppressing (high) polysulfide shuttling especially under high-sulfur-loading conditions (over 6 mg cm^{-2}). The current density was set at 1 mA cm^{-2} .

As shown in Figure 3, the presence of 2DSi (4 mg cm^{-2}) significantly affected the electrochemical behavior of CC (20 mg cm^{-2}) toward sulfur at an areal sulfur loading of 10 mg cm^{-2} . In addition, its catalytic effect is observed primarily on the lower plateau, which is relevant for the reduction reaction from high polysulfides (Li_2S_x , $4 < x \leq 8$) to low polysulfides (Li_2S_x , $1 \leq x \leq 4$) (Scheme S2). The corresponding second cathodic peak shifted by 100 mV to a higher potential value (2.08 V vs. Li/Li^+ ; Figure 3A) in the cyclic voltammogram (Figure 3A), and its cathodic current density simultaneously increased by 3.5 times from 0.33 to 1.14 mA cm^{-2} at a sweep rate of 0.01 mV s^{-1} . Similarly, the capacity generation from the lower plateau below 2.1 V versus Li/Li^+ increases from 1.7 to 3.9 mAh cm^{-2} with a significantly decreased polarization (187 vs. 360 mV), as shown in the GCPL results at 1 mA cm^{-2} (Figure 3B). With almost the same capacity generation from the higher plateau for both CC (2.5 mAh cm^{-2}) and 2DSi/CC (3.0 mAh cm^{-2}), the capacity ratio of the lower plateau to the higher plateau of the 2DSi/CC is calculated to be approximately 1.45, which corresponds to an enhancement factor of 200% as compared to that of CC (0.72). Consequently, the total sulfur utilization of CC at an areal sulfur loading of 10 mg cm^{-2} increases from 23.9% to 56.2% with the addition of 2DSi. In addition, the catalytic effect of the 2DSi on the lower plateau is maintained for over 200 charge/discharge cycles (Figure 3C), enabling stable LSBs with a high areal capacity of 7.49 mAh cm^{-2} and only a marginal degradation (0.14% loss per cycle). The performance values of the 2DSi/CC are comparable to the best values of high-loading-sulfur cathodes reported so far (Table S2).

The GCPL performance and the impedance of the 2DSi/CC are optimized (or saturated) at an areal loading of $4 \text{ mg 2DSi cm}^{-2}$ and 10 mg S cm^{-2} in the range between 2 and $6 \text{ mg 2DSi cm}^{-2}$ and between 2 and 15 mg S cm^{-2} , respectively (Figures S10–S12). In addition, different commercial current collectors (Al, CNT, and CC), generating different capacities from the higher plateau

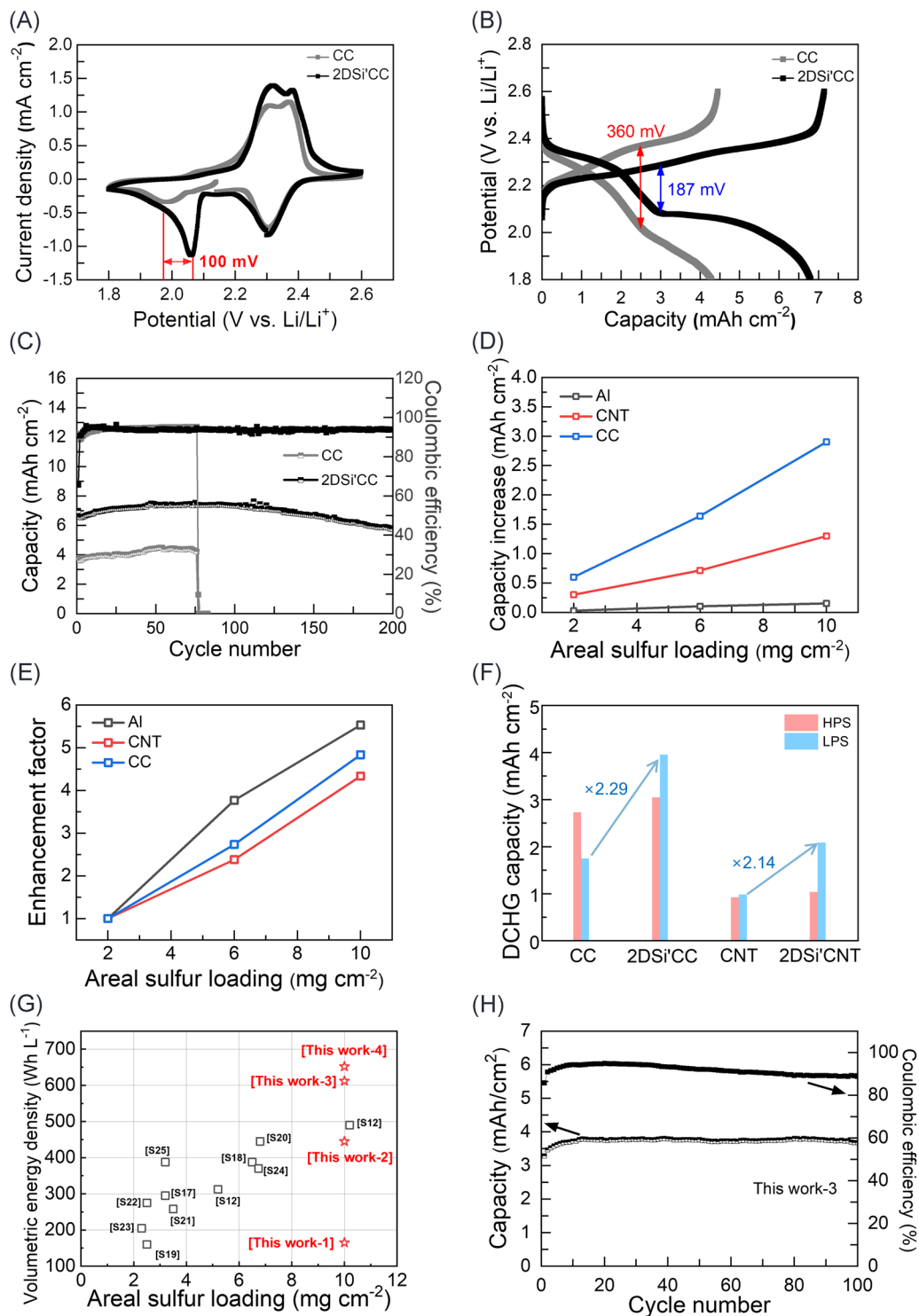


FIGURE 3 Electrochemical characterization of the 2DSi'CC at 10 mg S cm^{-2} : (A) CV diagrams at 0.01 mV s^{-1} , (B) 10th GCPL profiles at 1 mA cm^{-2} , and (C) cycle stability. Current collector-dependent GCPL performance at 1 mA cm^{-2} and 10 mg S cm^{-2} : (D) capacity increase versus areal sulfur loading, (E) enhancement factor versus areal sulfur loading, and (F) capacity generation from the lower (LPS) and higher plateau (HPS) during the discharge procedure. LSB cell using 2DSi'CNT and Super P pseudo-upper current collector: (G) Ragone plot and (H) cycle stability at 1 mA cm^{-2} and 10 mg S cm^{-2} . 2DSi, two-dimensional siloxene; CNT, carbon nanotube; CV, cyclic voltammetry; GCPL, galvanostatic cycling with potential limitation; LSB, lithium-sulfur battery

(0.05, 1.09, and 3.07 mAh cm⁻², respectively), display a similar enhancement of the areal capacity at areal sulfur loadings of 6 and 10 mg S cm⁻² as compared to that at 2 mg S cm⁻² (Figure 3D–F and S13). For example, the capacity generation from the lower plateau of both CC and CNT at an areal sulfur loading of 10 mg S cm⁻² increases approximately twofold with the addition of 2DSi, whereas that of the higher plateau remains almost constant with an increase of less than 10%. These results confirm the stoichiometric reactivity of the 2DSi, as well as its catalytic reactivity, which improves the efficiency of the 2DSi additive under high-sulfur-loading conditions. To this end, owing to (1) the low volume fraction of the void space and inactive carbons in the cathode (e.g., switching from CC to CNT), (2) lithium metal anode in slight excess of 10%, and (3) the Super P pseudo-upper current collector on the surface of the PP separator (0.8 mg cm⁻²), the volumetric energy density of LSB cells substantially increases from 157 Wh L_{cell}⁻¹ to 433 Wh L_{cell}⁻¹, and finally to 612 Wh L_{cell}⁻¹ at 1 mA cm⁻² in a coin cell or 652 Wh L_{cell}⁻¹ at 0.25 mA cm⁻² in a pouch cell (Figure 3G–H). At the different current rates, it shows good discharge capacity and capacity recovery of 5.9, 4.3, 2.8, and 1.9 mAh cm⁻² at different current densities of 0.25, 0.50, 0.75, and 1.00 mA cm⁻², respectively (Figure S23). The volumetric energy density of the LSB cells in this study is calculated based on the volume of all of the cell components including the Li metal anode, separator, sulfur, conductive carbon additive, polymer binder, carbon-based current collector, and 2DSi (see the Supporting Information for the calculation of volumetric energy density; Figure S14 and Calculation S3). Note that, except for 2DSi, we only use a commercial carbon-based current collector (CC or CNT) applicable for fabricating pouch-type cells, and thus, our method is suitable for industrial production. Combined with other well-designed carbon host materials, the performance of the cell increased significantly. A detailed explanation is provided in the next section on the mechanistic investigation of the chemical and electrochemical reactions between 2DSi and (high) polysulfides.

In addition to the electrochemical equilibrium, we investigated the electrochemical reaction kinetics of the 2DSi'CC using the power-law equation to verify the catalytic effect of 2DSi. The power-law dependence (*b* value) of the second cathodic peak current density (Figure S15) on the sweep rates changes from the kinetically fast surface-controlled process (CC, *b*₃ = 0.769) to the slow diffusion-controlled (2DSi'CC, *b*₃ at 2 mg S cm⁻² = 0.55, *b*₃ at 6 mg S cm⁻² = 0.58, and *b*₃ at 10 mg S cm⁻² = 0.64) Faradaic process in the scan rate range between 0.01 and 0.05 mV s⁻¹, whereas the *b*₂ of the first cathodic peak current density is maintained at approximately 0.8,

which is close to that of CC⁴⁵ (Figures S15 and S16). We attribute this to the significantly increased formation (or passivation) of insoluble lithium sulfide, leading to marked polarization enabled by 2DSi, which is consistent with the results of the equilibrium studies mentioned above. In addition, the *b*₃ value (0.641) of the second cathodic peak is lower than the *b*₂ value (0.879) of the first cathodic peak of the 2DSi'CC, suggesting that the liquid-to-solid reaction from high polysulfides to Li₂S₂/Li₂S must be the rate-determining step for the overall reduction reactions.⁴⁶ Furthermore, the 2DSi facilitates the sluggish electron/ion transfer for the liquid-to-solid reaction: (1) the *b*₃ value increases from 0.55 to 0.641, with an increase in the areal sulfur loading from 2 to 10 mg S cm⁻², (2) *R*_{ct}, *R*_b, and *R*_{SEI} of the 2DSi'CC remain low (less than 5 Ω) after cycling (Figure S17), and (3) the rate capability of the 2DSi'CC is superior to that of CC in the current density range between 1 and 4 mA cm⁻² (Figure S18).

3.4 | Role of 2DSi

The 2DSi facilitates more reduction reaction and thus generates increased capacity from the high polysulfides. The selective and reversible deposition of sulfur species on the 2DSi is confirmed by the XRD pattern, which reveals the reversible formation of Li₂S (JCPDS No. 01-077-2145, Figure 4A,B), and SEM images with elemental mapping, which reveals the uneven surface of the 2DSi due to the formation of sulfur-based material after discharge (Figure 4C,D). The surface deposition of sulfur species leads to a complete disappearance of the characteristic peak of the Si–Si bond in the Raman spectra of 2DSi at 1.5 V versus Li/Li⁺, which is reversibly recovered after removing the sulfur species at 3.0 V versus Li/Li⁺ (Figure 4E,F). In addition, the intercalation of the sulfur species into the interlayers of the 2DSi is evident from the disappearance of the (0 0 1) peak in the XRD patterns of the 2DSi after discharge (Figure 4D).

In addition, the CC-based LSB cells abruptly degrade after 77 cycles under the high-sulfur-loading conditions, which is prevented by the addition of 2DSi. Furthermore, the capacity generation from the lower plateau increased with an increase in the 2DSi areal loading from 2 to 6 mg 2DSi cm⁻² (Figure S10). The average increase in the lower plateau capacity induced by 2DSi was calculated to be 0.313 mAh mg_{2DSi}⁻¹. This result is consistent with the aforementioned experimental adsorption results (2.5 mmol_{Li2S6} mg_{2DSi}⁻¹) (see calculation details in the Supporting Information, Calculation S4). The adsorption of high polysulfides into 2DSi is an essential step in their electrochemical reaction, which indicates the heterogeneous (electro-)catalytic reaction. It is

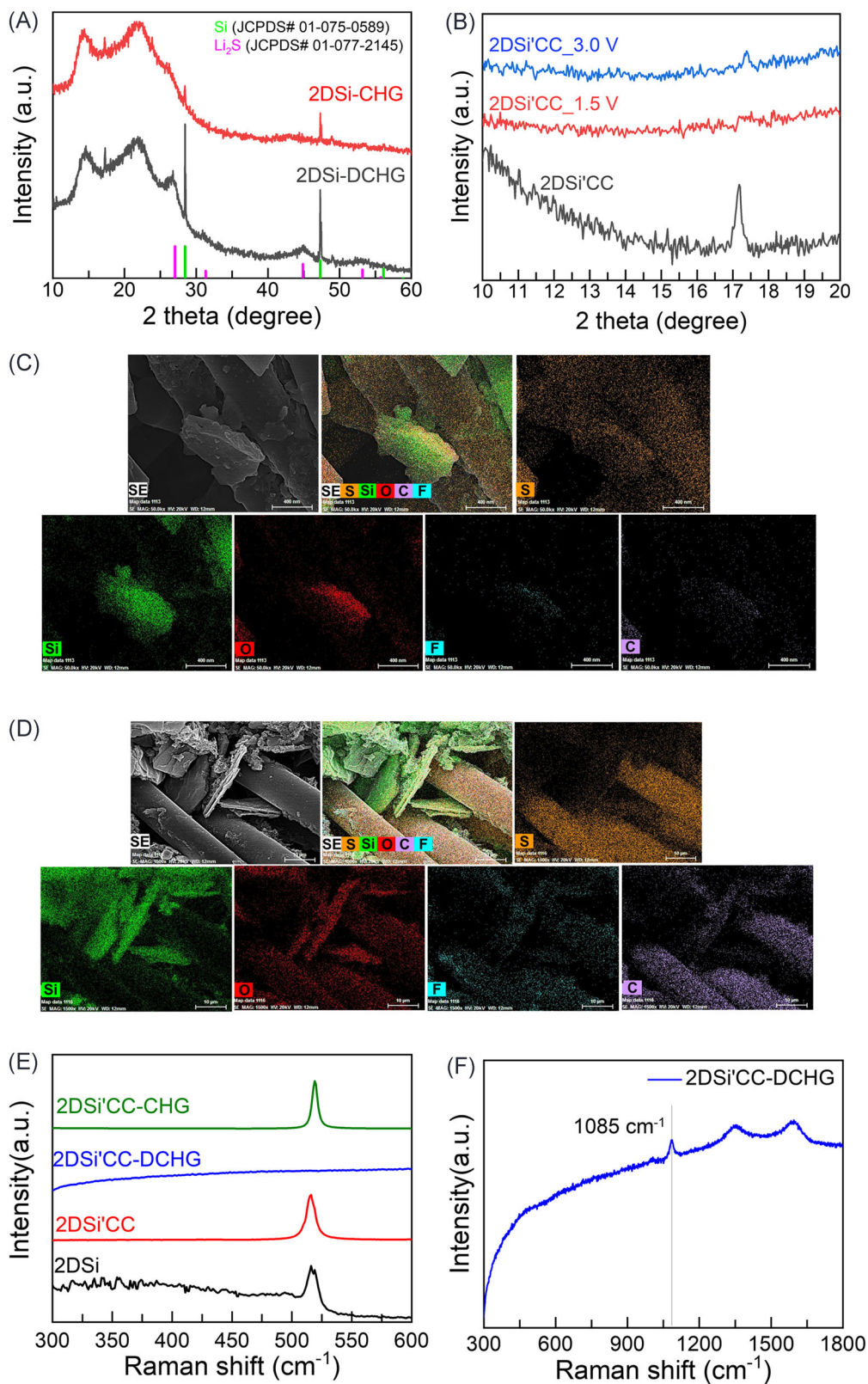


FIGURE 4 (A,B) XRD patterns of the 2DSi'CC after discharge to 1.5 V versus Li/Li^+ and charge to 3.0 V versus Li/Li^+ . (C) SEM and corresponding EDS mapping images of 2DSi'CC after discharge to 1.5 V versus Li/Li^+ and (D) charge to 3.0 V versus Li/Li^+ in the order of S, Si, O, F, and C. 2DSi'CC after the discharge and charge cycle. (E,F) Raman spectra of 2DSi'CC after discharging to 1.5 V versus Li/Li^+ and charging to 3.0 V versus Li/Li^+ . 2DSi, two-dimensional siloxene; CC, carbon cloth; EDS, energy dispersive spectroscopy; SEM, scanning electron microscopy; XRD, X-ray diffraction

noteworthy that the parent CaSi_2 (4 mg cm^{-2}) has no significant effect on the electrochemical behavior of CC toward sulfur, indicating that such (electro-)catalytic sites emerge after the extraction of Ca^{2+} (Figure S19).

One possible explanation for the enhancement in the electrochemical performance of CC toward sulfur is that the polysulfide shuttling is impeded by the 2DSi additive owing to its strong affinity to polysulfides combined with the confinement effect (Scheme S3). The potential-wise high-resolution S 2p XPS spectra reveal that the 2DSi retains the polysulfides' emerging multiple peaks at 160–164 eV (Figure 5A), whereas these sulfur species are completely absent in the XPS spectra of the CC cycled without 2DSi (Figure 5B) in the potential range between 1.5 and 3.0 V versus Li/Li^+ . We believe that this is because the surficial sulfur species on the CC electrode were washed away during the sample preparation, whereas those on the 2DSi/CC electrode were robustly retained, indicating the strong affinity between 2DSi and polysulfides. This is consistent with the photo images of the cycled Li metal with the

separator revealing a significant decrease in the dissolution of yellow polysulfides in the 2DSi/CC electrode (Figure S20). In addition, with an increase in the cell potential from 1.5 to 3.0 V versus Li/Li^+ , the areal contribution of the peak for the central S at approximately 164 eV (S_B^0) increased from 7.61% to 29.41% and that for the terminal S at approximately 163 eV (S_T^{-1}) decreased from 32.04% to 7.00% (Figure 5C). This indicates that the polysulfides retained by 2DSi are active in the reversible, step-wise redox reaction during cycling (Figure 5A).

The effective interaction between the 2DSi and polysulfides was also confirmed by density functional theory (DFT) calculations (Figure S21). The binding energy of Li_2S_4 , as a representative of lithium polysulfide, on a flawless 2DSi surface was -2.14 eV , which is similar to that on the TiS_2 , a moderate anchoring material.⁴⁷ On a defective surface exposing the undercoordinated Si atoms without a OH functional, the binding of Li_2S_4 was strengthened to -3.87 eV . These moderate interactions between 2DSi and polysulfides, regardless of the surface

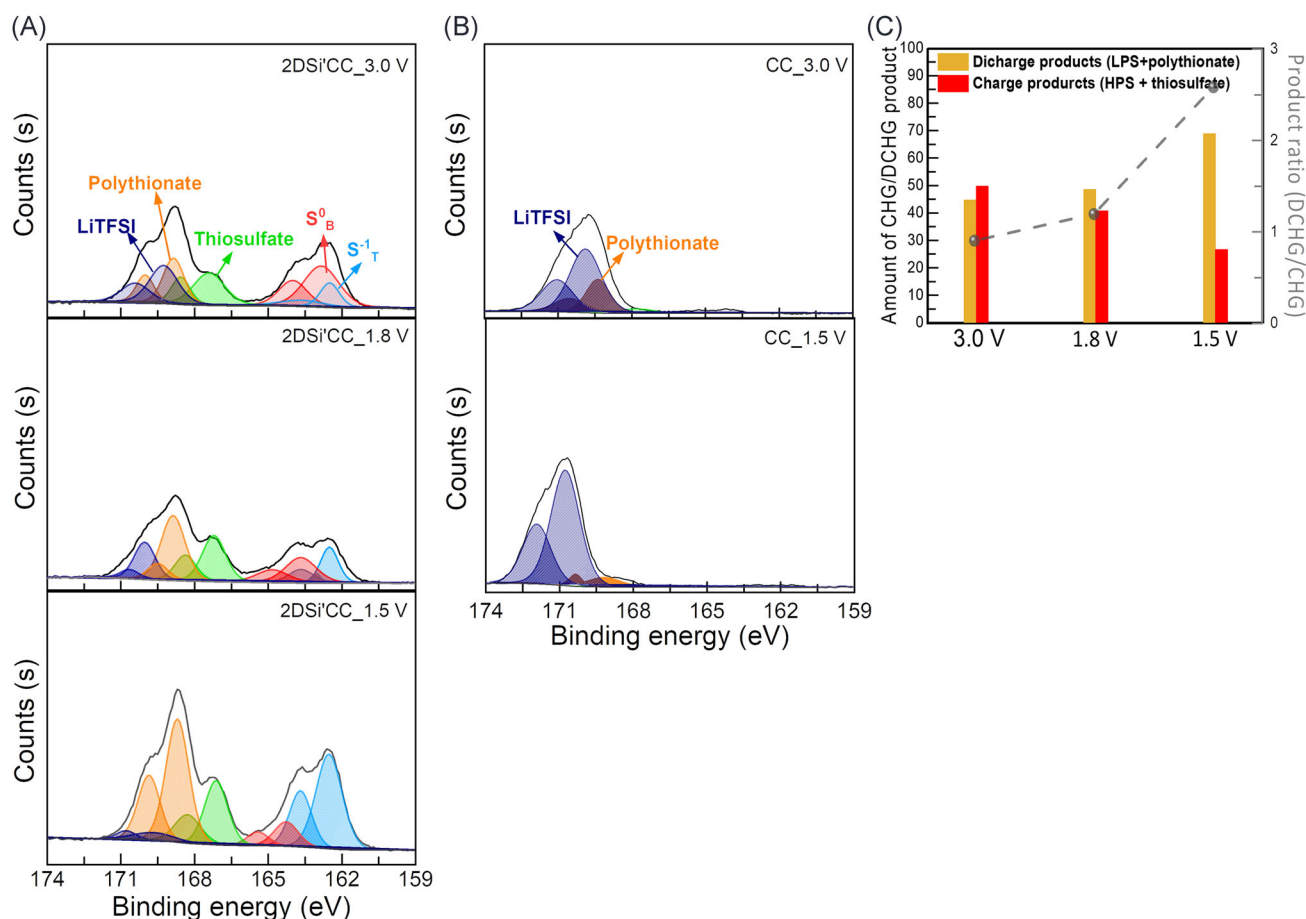
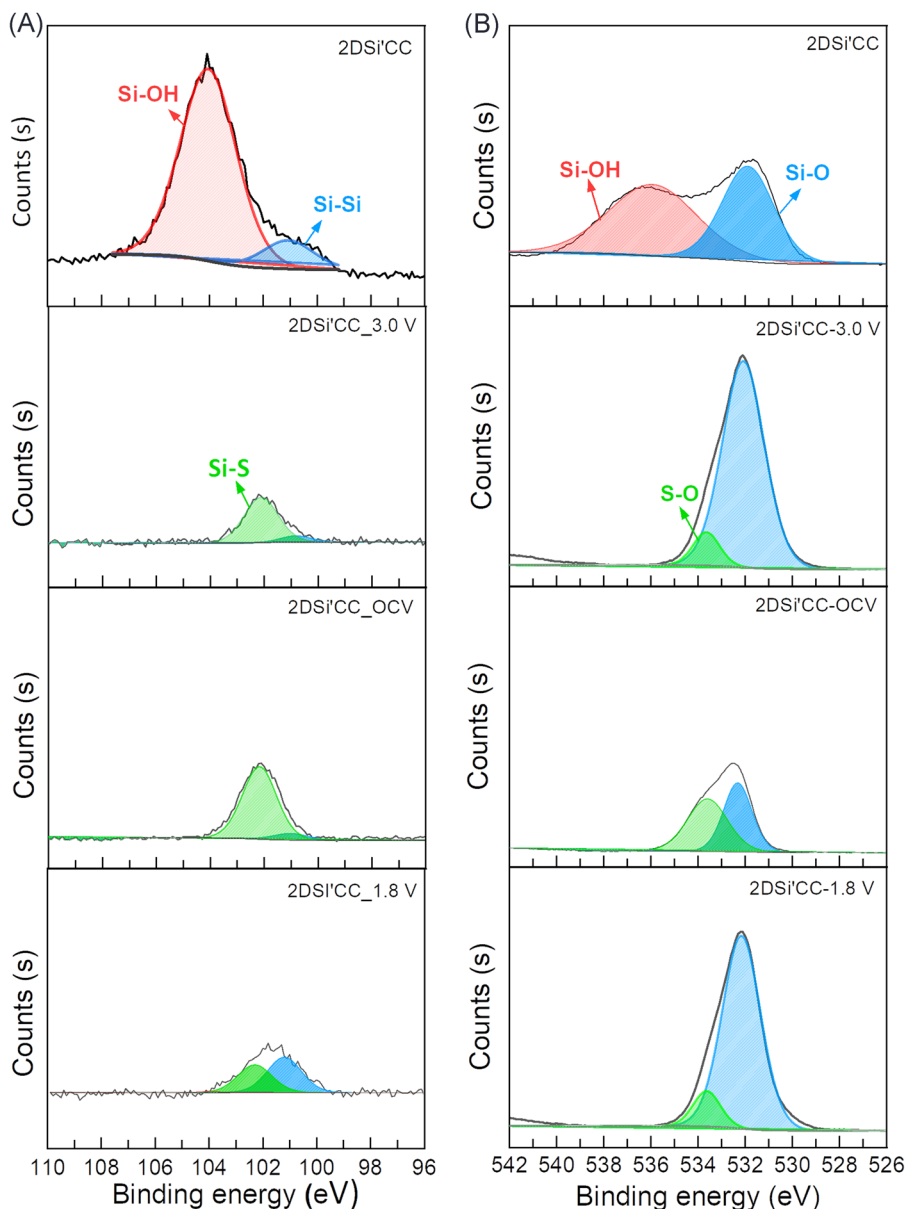


FIGURE 5 Potential-wise high-resolution XPS spectra of (A) 2DSi/CC and (B) CC. (C) Portion of discharge (LPS + polythionate) and charge (HPS + thiosulfate) products at 1.5, 1.8, and 3.0 V versus Li/Li^+ . 2DSi, two-dimensional siloxene; CC, carbon cloth; HPS, high plateau surface; LPS, low plateau surface; XPS, X-ray photoelectron spectrometry

FIGURE 6 Potential-wise high-resolution XPS spectra of the 2DSi/CC: (A) Si 2p and (B) O1s. 2DSi, two-dimensional siloxene; CC, carbon cloth; XPS, X-ray photoelectron spectrometry



state, indicate that the 2DSi can be an effective additive for retaining polysulfides.

Another remarkable observation in the XPS spectra is the sulfur peaks between 166 and 170 eV (Figure 5A,B). The binding energies at 167 and 169 eV can be assigned to thiosulfate and polythionate, respectively, and they are conspicuous only in the presence of 2DSi. Previous studies have reported that the electrochemical formation of thiosulfate and polythionate increased the affinity of the electrode to polysulfides, thus improving battery performance. In addition, these studies reported that thiosulfate formation requires redox potential of higher than 2.4 V versus Li/Li⁺, which corresponds to the onset of the sulfur reduction, to have a more thermodynamic preference in thiosulfate formation than the reduction of polysulfides. Adsorption of Li on the 2DSi surface,

however, was calculated to have lower redox potential (~1 V vs. Li/Li⁺) than this onset potential, implying that the reduction of polysulfide will begin ahead of the electrochemical formation of thiosulfates. Thus, the observed thiosulfate in the 2DSi might have a different formation mechanism than the previously suggested redox-based thiosulfate. In addition, the thiosulfate and polythionate signals are significant in both the charged and discharged states of the 2DSi/CC electrode. This implies that a part of thiosulfate and polythionate are chemically formed in the absence of the electrochemical process. According to a previous study, abundant surface hydroxyl groups on the surface of 2DSi can react with polysulfides to generate insoluble thiosulfate.²¹ As evidence, the oxidation of polysulfides (Li₂S₆) was initiated upon contact with the 2DSi even at an open-circuit

voltage (OCV) without applying current. Consistently, the S–O peak reflecting the thiosulfate was observed in the O 1s XPS spectrum at OCV (Figure S22). This chemical interaction between S and O was further confirmed by comparing the O 1s XPS spectra of 2DSi/CC before and after the cell fabrication. In the bare 2DSi/CC (Figure 6A), an obvious peak was observed at 536 eV corresponding to Si–OH, which disappeared after fabricating the cell. This result suggests that the surface OH groups are consumed by interaction with polysulfides, although its detailed mechanism is still unclear. The electrochemical formation of thiosulfate and polythionate was also observed in the XPS results as their signals increased during the discharge from 3.0 to 1.8 V versus Li/Li⁺.

This series of reactions facilitates the conversion of the soluble polysulfides into insoluble lithium sulfide, thus reducing the loss of active sulfur species caused by dissolution. Notably, the thiosulfate formation further strengthens the interaction of 2DSi with polysulfides by revealing a fresh Si surface. In addition, the nucleophilic sulfur species donate electrons to the Si atoms with unoccupied orbitals, leading to the formation of coordination compounds, as confirmed by the newly observed peak of Si–S bond at 102 eV in the high-resolution XPS Si 2p spectra (Figure 6B).²¹ Furthermore, the areal ratio of polythionate plus terminal S (or products) to that of thiosulfate plus central S (or reactants) gradually increases with decreasing cell potential during the discharge procedure. This interplay confirms the electrochemical activity of the *in-situ* formed thiosulfate/polythionate redox couple and the resulting Si surface toward polysulfides in their chemical binding and conversion into lithium sulfide under redox conditions.

4 | CONCLUSION

In summary, we showed that a 2DSi is highly effective in immobilizing and utilizing the intermediate polysulfides, especially under high-sulfur-loading conditions. The 2DSi was modified to have a layered structure decorated with vertically aligned surface hydroxyl groups by solvent extraction at RT. The stoichiometric reaction with polysulfides induced hydroxyl-rich, layered 2DSi electrocatalytic activity based on the thiosulfate/polythionate redox couple with a confinement effect via intercalation, and catalytic surface affinity based on the Lewis acid–base interaction, which optimized the performance of the 2DSi at a 1:2.5 2DSi:sulfur weight ratio. With these multiple effects, the 2DSi improves the conversion from high polysulfides into low polysulfides or lithium sulfide of the cathode, thereby increasing the capacity

generation from the lower plateau and cycle stability at 1 mA cm⁻¹ and ~10 mg S cm⁻¹. Combined with commercial carbon materials as a sulfur supporting material and a current collector, the 2DSi-based LSB cells delivered a high areal capacity (7.49 mAh cm⁻¹) and a high volumetric energy density (612 Wh L_{cell}⁻¹) with marginal capacity loss (0.12%–0.14% loss per cycle).

ACKNOWLEDGMENTS

This study was financially supported by the R&D Convergence Program of NST (National Research Council of Science & Technology) of the Republic of Korea (CAP-15-02-KBSI), a National Research Foundation of Korea (NRF) grant funded by the Korean Government (MSIT) (no. 2019R1C1C1007745), and a National Research Foundation of Korea (NRF) grant funded by the Korean Government (Ministry of Science, ICT & Future Planning) (no. 2019R1A4A2001527).

CONFLICT OF INTEREST

The authors declare no conflict of interest.

DATA AVAILABILITY STATEMENT

Supporting Information is available from the Wiley Online Library or from the author.

ORCID

Hui-Ju Kang  <https://orcid.org/0000-0003-2735-1161>

Jae-Woo Park  <https://orcid.org/0000-0002-7916-6809>

Hyun Jin Hwang  <https://orcid.org/0000-0001-7163-018X>

Heejin Kim  <https://orcid.org/0000-0003-3027-6983>

Kwang-Suk Jang  <https://orcid.org/0000-0001-5835-9364>

Xiulei Ji  <https://orcid.org/0000-0002-4649-9594>

Hae Jin Kim  <https://orcid.org/0000-0002-1960-0650>

Won Bin Im  <https://orcid.org/0000-0003-2473-4714>

Young-Si Jun  <https://orcid.org/0000-0002-7157-4920>

REFERENCES

1. Liu Y-T, Liu S, Li G-R, Yan T-Y, Gao X-P. High volumetric energy density sulfur cathode with heavy and catalytic metal oxide host for lithium–sulfur battery. *Adv Sci.* 2020;7(12):1903693.
2. Balogun M-S, Yang H, Luo Y, et al. Achieving high gravimetric energy density for flexible lithium-ion batteries facilitated by core–double-shell electrodes. *Energy Environ Sci.* 2018;11(7):1859-1869.
3. Divya KC, Ostergaard J. Battery energy storage technology for power systems—an overview. *Electr Power Syst Res.* 2009;79(4):511-520.
4. Ulvestad A. A brief review of current lithium-ion battery technology and potential solid-state battery technologies. *arXiv: Appl Phys.* 2018;1803:04317.

5. Fan X, Liu B, Liu J, et al. Battery technologies for grid-level large-scale electrical energy storage. *Trans Tianjin Univ.* 2020; 26(2020):92-103.
6. Eucar.be. Battery requirements for future automotive applications. <https://www.eucar.be/battery-requirements-for-future-automotive-applications/>. May 20, 2020.
7. Kim JH, Lee YH, Cho SJ, et al. Nanomat Li-S batteries based on all-fibrous cathode/separator assemblies and reinforced Li metal anodes: towards ultrahigh energy density and flexibility. *Energy Environ Sci.* 2019;12(1):177-186.
8. Yuan Z, Peng HJ, Huang JQ, et al. Hierarchical free-standing carbon-nanotube paper electrodes with ultrahigh sulfur-loading for lithium-sulfur batteries. *Adv Funct Mater.* 2014; 24(39):6105-6112.
9. Qie L, Manthiram A. High-energy-density lithium-sulfur batteries based on blade-cast pure sulfur electrodes. *ACS Energy Lett.* 2016;1(1):46-51.
10. Chung SH, Manthiram A. Rational design of statically and dynamically stable lithium-sulfur batteries with high sulfur loading and low electrolyte/sulfur ratio. *Adv Mater.* 2018; 30(6):1705951.
11. Chung S-H, Chang C-H, Manthiram A. Hierarchical sulfur electrodes as a testing platform for understanding the high-loading capability of Li-S batteries. *J Power Sources.* 2016;334: 179-190.
12. Peng HJ, Huang JQ, Cheng XB, Zhang Q. Review on high-loading and high-energy lithium-sulfur batteries. *Adv Energy Mater.* 2017;7(24):1700260.
13. Chung SH, Chang CH, Manthiram A. A carbon-cotton cathode with ultrahigh-loading capability for statically and dynamically stable lithium-sulfur batteries. *ACS Nano.* 2016; 10(11):10462-10470.
14. Xue W, Shi Z, Suo L, et al. Intercalation-conversion hybrid cathodes enabling Li-S full-cell architectures with jointly superior gravimetric and volumetric energy densities. *Nat Energy.* 2019;4(2019):374-382.
15. Kang N, Lin Y, Yang L, et al. Cathode porosity is a missing key parameter to optimize lithium-sulfur battery energy density. *Nat Commun.* 2019;10:4597.
16. Elwinger F, Pourmand P, Furó I. Diffusive transport in pores. Tortuosity and molecular interaction with the pore wall. *J Phys Chem C.* 2017;121(25):13757-13764.
17. He G, Evers S, Liang X, Cuisinier M, Garsuch A, Nazar LF. Tailoring porosity in carbon nanospheres for lithium-sulfur battery cathodes. *ACS Nano.* 2013;7(12):10920-10930.
18. Liang X, Garsuch A, Nazar LF. Sulfur cathodes based on conductive MXene nanosheets for high-performance lithium-sulfur batteries. *Angew Chem Int Ed.* 2015;54(13):3907-3911.
19. Liang X, Kwok CY, Lodi-Marzano F, et al. Tuning transition metal oxide-sulfur interactions for long-life lithium-sulfur batteries: the "Goldilocks" principle. *Adv Energy Mater.* 2016; 6(6):1501636.
20. Sun Z, Zhang J, Yin L, et al. Conductive porous vanadium nitride/graphene composite as chemical anchor of polysulfides for lithium-sulfur batteries. *Nat Commun.* 2017;8: 14627.
21. Liang X, Rangom Y, Kwok CY, Pang Q, Nazar LF. Interwoven MXene nanosheet/carbon-nanotube composites as Li-S cathode hosts. *Adv Mater.* 2017;29(3):1603040.
22. Liang X, Hart C, Pang Q, Garsuch A, Weiss T, Nazar LF. A highly efficient polysulfide mediator for lithium-sulfur batteries. *Nat Commun.* 2015;6:5682.
23. Alhabebe M, Maleski K, Anasori B, et al. Guidelines for synthesis and processing of two-dimensional titanium carbide ($Ti_3C_2T_x$ MXene). *Chem Mater.* 2017;29:7633-7644.
24. Hu G, Xu C, Sun Z, et al. 3D graphene-foam-reduced-graphene-oxide hybrid nested hierarchical networks for high-performance Li-S batteries. *Adv Mater.* 2016;28(8):1603-1609.
25. Oh SY, Imagawa H, Itahara H. Si-based nanocomposites derived from layered $CaSi_2$: influence of synthesis conditions on the composition and anode performance in Li-ion batteries. *J Mater Chem A.* 2014;2(31):12501-12506.
26. Wöhler F. Ueber verbindungen des siliciums mit sauerstoff und wasserstoff. *Justus Liebigs Ann Chem.* 1863;127(3):257-274.
27. Khodaveisi J, Banejad H, Afkhami A, Olyae E, Lashgari S, Dashti R. Synthesis of calcium peroxide nanoparticles as an innovative reagent for in situ chemical oxidation. *J Hazard Mater.* 2011;192(3):1437-1440.
28. Zhang C, Lv W, Xie XY, Tang DM, Liu C, Yang QH. Towards low-temperature thermal exfoliation of graphite oxide for graphene production. *Carbon.* 2013;62:11-24.
29. Yamanaka S, Matsu-ura H, Ishikawa M. New deintercalation reaction of calcium from calcium disilicide. Synthesis of layered polysilane. *Mater Res Bull.* 1996;31(3):307-316.
30. Imagawa H, Itahara H. Stabilized lithium-ion battery anode performance by calcium-bridging of two-dimensional siloxene layers. *Dalton Trans.* 2017;46(11):3655-3660.
31. Fuchs HD, Stutzmann M, Brandt MS, et al. Porous silicon and siloxene: vibrational and structural properties. *Phys Rev B.* 1993;48(11):8172-8189.
32. Dettlaff-Weglikowska U, Hönle W, Molassioti-Dohms A, Finkbeiner S, Weber J. Structure and optical properties of the planar silicon compounds polysilane and Wohler siloxene. *Phys Rev B.* 1997;56(20):13132-13140.
33. Ali MA, Tchalala MR. Chemical synthesis of silicon nanosheets from layered calcium disilicide. *J Phys: Conf Ser.* 2014;491:012009.
34. Tchalala MR, Ali MA, Enriquez H, et al. Silicon sheets by redox assisted chemical exfoliation. *J Condens Matter Phys.* 2013;25(44):442001.
35. van de Walle CG, Northrup JE. First-principles investigation of visible light emission from silicon-based materials. *Phys Rev Lett.* 1993;70(8):1116-1119.
36. Armin W, Gerd B, Heinrich M. The topochemical reaction of $CaSi_2$ to a two-dimensional subsiliceous acid $Si_6H_3(OH)_3$ (=Kautskys' Siloxene). *Z Naturforsch B.* 1980; 35(1):25-30.
37. Xin S, Gu L, Zhao N-H, et al. Smaller sulfur molecules promise better lithium-sulfur batteries. *J Am Chem Soc.* 2012; 134(45):18510-18513.
38. Peng Z, Fang W, Zhao H, et al. Graphene-based ultrathin microporous carbon with smaller sulfur molecules for excellent rate performance of lithium-sulfur cathode. *J Power Sources.* 2015;282:70-78.
39. Li Z, Yuan L, Yi Z, et al. Insight into the electrode mechanism in lithium-sulfur batteries with ordered microporous carbon confined sulfur as the cathode. *Adv Energy Mater.* 2014;4(7):1301473.

40. Zheng S, Wen Y, Zhu Y, et al. In situ sulfur reduction and intercalation of graphite oxides for Li-S battery cathodes. *Adv Energy Mater.* 2014;4(16):1400482.
41. Ma S, Islam SM, Shim Y, et al. Highly efficient iodine capture by layered double hydroxides intercalated with polysulfides. *Chem Mater.* 2014;26(24):7114-7123.
42. Zhou G, Zhao S, Wang T, et al. Theoretical calculation guided design of single-atom catalysts toward fast kinetic and long-life Li-S batteries. *Nano Lett.* 2020;20(2):1252-1261.
43. Song J-Y, Lee H-H, Hong WG, et al. A polysulfide-infiltrated carbon cloth cathode for high-performance flexible lithium-sulfur batteries. *Nanomaterials.* 2018;8(2):90.
44. Yamin H, Gorenstein A, Penciner J, Sternberg Y, Peled E. Lithium-sulfur battery. *J Electrochem Soc.* 1988;135(5):1045-1048.
45. Shi W, Li Y, Liu Z, et al. Highly stable lithium-sulfur batteries promised by siloxene: an effective cathode material to regulate the adsorption and conversion of polysulfides. *Adv Funct Mater.* 2020;30(12):1910331.
46. Tao Y, Wei Y, Liu Y, et al. Kinetically-enhanced polysulfide redox reactions by Nb₂O₅ nanocrystals for high-rate lithium-sulfur battery. *Energy Environ Sci.* 2016;9(10):3230-3239.
47. Zhang Q, Wang Y, Seh ZW, Fu Z, Zhang R, Cui Y. Understanding the anchoring effect of two-dimensional layered materials for lithium-sulfur batteries. *Nano Lett.* 2015;15(6):3780-3786.

SUPPORTING INFORMATION

Additional Supporting Information may be found online in the supporting information tab for this article.

How to cite this article: Kang H-J, Park J-W, Hwang HJ, et al. Electrocatalytic and stoichiometric reactivity of 2D layered siloxene for high-energy-dense lithium-sulfur batteries. *Carbon Energy.* 2021;3:976-990.
<https://doi.org/10.1002/cey2.152>